Metastable materials solidified from undercooled melts

2001 J. Phys.: Condens. Matter 13 7737

(http://iopscience.iop.org/0953-8984/13/34/317)

INSTITUTE OF PHYSICS PUBLISHING JOURNAL OF PHYSICS: CONDENSED MATTER

J. Phys.: Condens. Matter **13** (2001) 7737–7751 PII: S0953-8984(01)24199-X

Metastable materials solidified from undercooled melts

Dieter M Herlach

Institut für Raumsimulation, DLR, D-51170 Köln, Germany

E-mail: Dieter.Herlach@dlr.de

Received 24 April 2001
Published 9 August 2001
Online at stacks.iop.org/JPhysCM/13/7737

Abstract

Techniques of containerless processing are applied to undercool and solidify metals and alloys. These techniques allow direct measurements of both the undercooling and the crystal growth velocity. Experimental results are presented for studies of nucleation of metastable crystalline phases and quasicrystals. Measurements of the dendrite growth velocity as a function of undercooling are exemplified for dilute Ni-based alloys and intermetallics. The results are analysed within current theories of rapid crystal growth. Their consequences on the formation of grain refined microstructures are highlighted. In addition, recent experiments on the undercooling of magnetic alloys are discussed, revealing the existence of long-range magnetic ordering in an undercooled melt.

1. Introduction

In the past, rapid quenching methods have been successfully applied to produce metastable solids from the liquid state. A great variety of metastable materials have been discovered, with physical properties which make them suitable as new high-performance materials in mechanical and electrical engineering. To date, such metastable solids are even being produced on an industrial scale for their application in, e.g., steel production, design of electronic devices and aerospace applications. In order to develop a predictive capability for modes of metastable solidification, recent efforts concentrate on the understanding, description and modelling of the physical mechanisms [1] relevant to the formation of metastable phases from the liquid state. From a thermodynamic point of view, the undercooling of the melt is a necessary precondition for the solidification of metastable phases.

The present work reports on direct experimental investigations of both nucleation and dendrite growth in bulk undercooled melts of metals and alloys, and their impact on the formation of metastable materials. Undercooling phenomena in melts of quasicrystal forming alloys are studied with respect to a possible influence of polytetrahedral short-range order in the state of the undercooled melt on the nucleation barrier. Furthermore, it is demonstrated that, provided that the melt is sufficiently undercooled prior to solidification, the nucleation

of a metastable bcc phase in the Fe–Ni–Cr alloy system is possible even in the concentration range where the fcc phase is stable.

Direct measurements of dendrite growth velocities as a function of undercooling are presented for dilute Ni–B alloys and the intermetallic compound $Co_{50}Si_{50}$. They allow for a detailed study of solute trapping and disorder trapping during rapid solidification of deeply undercooled metals. These mechanisms are crucial for the solidification of metastable supersaturated solutions and disordered superlattice structures in intermetallics. Metastability is also present in grain refined materials. The excess free energy of the undercooled melt can be used by the system to build up very fine grains in diameter of 1 μm or even less.

Finally, experiments will briefly be introduced in which metallic melts of Co–Pd are undercooled to their magnetic transition temperatures. The onset of magnetic ordering is evidenced by measurements of the magnetization and by muon-spin-rotation spectroscopy. It is shown that the onset of magnetic ordering may stimulate the crystal nucleation of undercooled melts.

2. Experimental details

Samples having a mass of about 1 g were prepared from the constituents of purity better than 99.99% by premelting in an induction furnace into spheres of about 6 mm diameter. Undercooling conditions were established by the application of the electromagnetic levitation technique. The experiments were performed under high-purity environmental conditions. Temperatures were measured contactlessly by pyrometry. For further details of the experimental methods and a review of the application of containerless processing in the study of undercooled melts see [2].

3. Nucleation of quasicrystalline and crystalline phases

3.1. Quasicrystalline structures

Nucleation into a specific crystallographic phase is characterized by an activation energy ΔG^* to form a nucleus of critical size in the undercooled melt. The nucleation barrier arises from the interfacial energy σ_{sl} between the crystal nucleus and the undercooled melt. According to classical nucleation theory [3] and to the negentropic model by Spaepen [4] for the estimation of σ_{sl}, ΔG^* reads

$$\Delta G^* = \frac{16\pi r^3}{3\Delta G^2} f(\theta) \qquad \text{with } \sigma_{sl} = \alpha_s \frac{\Delta S_f}{N_A^{1/3} V_m^{2/3}} T. \tag{1}$$

$f(\theta)$ is a catalytic potency factor in the case of heterogeneous nucleation, ΔG the Gibbs free energy difference between the solid and the liquid phase, ΔS_f the entropy of fusion, N_A the Avogadro number, V_m the molar volume, T the temperature and α_s a factor depending on the structure of the nucleus with numerical values $\alpha_s = 0.71$ for a bcc, and $\alpha_s = 0.86$ for a fcc or hcp structure, respectively.

Hence, the barrier for nucleation, i.e. the interfacial energy σ_{sl}, depends on the structure of the nucleus. σ_{sl} is smaller for systems with similar short-range order of the undercooled melt and the nucleus. Already Frank has pointed out that an icosahedral short-range order should be energetically favoured in undercooled melts of metals and metallic alloys [5]. Hence, the energy barrier between an undercooled melt and a nucleus of a crystallographic phase with polytetrahedral symmetry should be small in comparison to crystalline phases.

The interfacial energy is often determined by measuring the maximum undercooling attainable for a melt [6]. Undercooling experiments on alloys which form quasicrystalline phases have been performed using the electromagnetic levitation technique [7]. Figure 1 shows two temperature–time profiles obtained from experiments on an $Al_{60}Cu_{34}Fe_6$ alloy which forms an icosahedral (I) phase (right), and on an $Al_{65}Cu_{25}Co_{10}$ alloy which solidifies in a decagonal (D) phase (left).

Similar experiments were conducted on the crystalline alloys $Al_{13}Fe_4$ and Al_5Fe_2, which form Frank–Kasper phases characterized by unit cells of different sizes (100 atoms in the λ-$Al_{13}Fe_4$ phase and 15 atoms in the μ-Al_5Fe_2 phase, respectively) with polytetrahedral symmetry elements [7, 8]. The results of all these undercooling experiments have been analysed within the classical nucleation theory [3]. Assuming that a single nucleation event is sufficient to initiate solidification, and supposing that nucleation is homogeneous, the following sequence of interfacial energies has been deduced according to equation (1):

$$\sigma_I = 0.091 \text{ J m}^{-2} < \sigma_D = 0.112 \text{ J m}^{-2} < \sigma_\lambda = 0.159 \text{ J m}^{-2} < \sigma_\mu = 0.186 \text{ J m}^{-2} \qquad (2)$$

with σ_I, σ_λ, σ_μ, and σ_D the interfacial energies of icosahedral (I) phase, λ- and μ-phases of quasicrystalline approximants and decagonal (D) phase, respectively, all of them smaller than, e.g., $\sigma = 0.464$ J m^{-2} for a crystalline Ni nucleus of fcc structure. This sequence indicates that an icosahedral short-range order is present in undercooled metallic melts which favours the solidification of solid phases having polytetrahedral symmetry elements. The more pronounced the polytetrahedral symmetry, the lower the nucleation barrier and, hence, the maximum undercoolability. The present analysis is based upon the assumption of homogeneous nucleation. Atomization and drop-tube experiments on Al–Mn quasicrystal forming alloys indicate that there is a high probability for quasicrystalline phases to be formed by homogeneous nucleation or heterogeneous nucleation of very small catalytic potency ($f(\theta) \approx 1$) in containerlessly undercooled melts [9, 10]. If, nevertheless, heterogeneous nucleation is tentatively assumed this would have the following consequences: anticipating the same catalytic potency $f(\theta)$ for all phases the main conclusions remain unchanged. On the other hand, if the observed change of ΔG^* is exclusively attributed to a change in $f(\theta)$ an anomalous variation has to be postulated, i.e. by a factor of three between the two quasicrystalline phases and even higher values between the icosahedral and crystalline phases [7].

3.2. Crystalline structures

The dependence of the activation energy on the crystallographic structure of the nucleus has a strong impact on the solidification of metastable phases. As has been shown by studies on the model system Fe–Ni, a metastable bcc phase crystallizes even in the concentration regime where the fcc phase is stable, provided a critical undercooling is exceeded [11]. The critical undercooling for metastable bcc solidification rapidly increases with Ni concentration so that at concentrations larger than 10 at.% Ni the achievable undercoolings are not sufficiently high to primarily solidify the metastable bcc phase. But even in this concentration range metastable bcc crystallization is possible when using the method of externally stimulated heterogeneous nucleation of metastable bcc phase. In this case the Fe–Ni melt is undercooled and subsequently touched by a nucleation trigger needle made of a $Fe_{95}Mo_5$ alloy. This material shows a stable high temperature phase with a structure throughout similar to the metastable bcc phase in Fe–Ni. In such a way the heterogeneous nucleation of bcc solidification is catalysed in undercooled Fe–Ni melts [12]. Figure 2 illustrates both the principle of experimental procedure (left-hand side) and the temperature-time profiles recorded for spontaneous and triggered nucleation

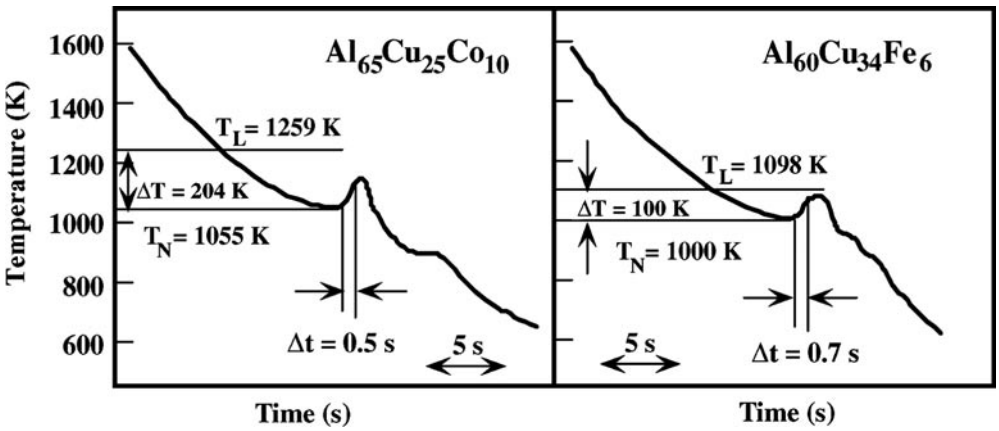

Figure 1. Temperature-time profiles, obtained from levitation undercooling experiments on quasicrystal forming alloys: left, $Al_{65}Cu_{25}Co_{10}$, forming a decagonal D phase; right, $Al_{60}Cu_{34}Fe_6$ forming an icosahedral I phase.

(right hand side). The primary crystallization of metastable bcc phase in $Fe_{76}Ni_{24}$ alloy is observed by a temperature rise upon recalescence up to the virtual melting temperature of metastable bcc phase, $T_l^{\delta} = 1690$ K. T_l^{δ} is smaller than the liquidus temperature of stable fcc phase, $T_l^{\gamma} = 1751$ K, up to which the temperature rises during spontaneous crystallization. The primarily formed metastable bcc phase transforms into stable fcc phase upon cooling of the as-solidified sample as indicated by the small hump superimposed to the temperature-time profile in case of triggered nucleation. As a consequence the formation of the metastable bcc phase is evidenced by x-ray diffraction on these samples at room temperature.

According to equation (1) the results on metastable bcc-form formation in Fe–Ni melts can be understood by a smaller activation energy to form critical nuclei of metastable bcc crystallites either by the smaller structural factor α in the interfacial energy σ as observed during spontaneous crystallization of deeply undercooled Fe-rich Fe–Ni alloys or by a large reduction of the catalytic potency factor $f(\theta)$ of heterogeneous nucleation of bcc phase on more concentrated Fe–Ni alloys due to external nucleation triggering.

Similar results of the formation of metastable bcc phase have been obtained from analogous studies on the ternary alloy system Fe–Ni-Cr [13, 14]. This alloy exhibits a phase competition of ferritic (bcc) and austenitic (fcc) phase which is similar to the one observed in the binary Fe–Ni system. However, it is of more practical relevance as a basic system for steel production. Also binary Ni–V alloys have been investigated with respect to phase selection through undercooling. Ni–V alloys show a phase competition between three different crystallographic phases of bcc and fcc structure and, in addition, an intermetallic σ' phase with a large unit cell consisting of 32 atoms. Also in this case, a preference of metastable bcc phase is observed in direct competition to fcc phase provided the undercooling exceeds a critical value depending on composition [15]. The σ' phase of Ni–V alloy is of special interest. It shows a tetrahedral short range order in its unit cell similar to that of quasicrystal forming alloys. Since phases of tetrahedral short range order should possess a small interfacial energy (see discussion of quasicrystals) ΔG^* is expected to be small [16]. The crystallization of the σ' phase, therefore, should be favoured compared with the phases of cubic structure. Surprisingly, this is in contrast to the experiments. Detailed studies of phase selection processes in undercooled melts of Ni–V alloys by energy dispersive x-ray diffraction using synchrotron radiation [17] clearly show the

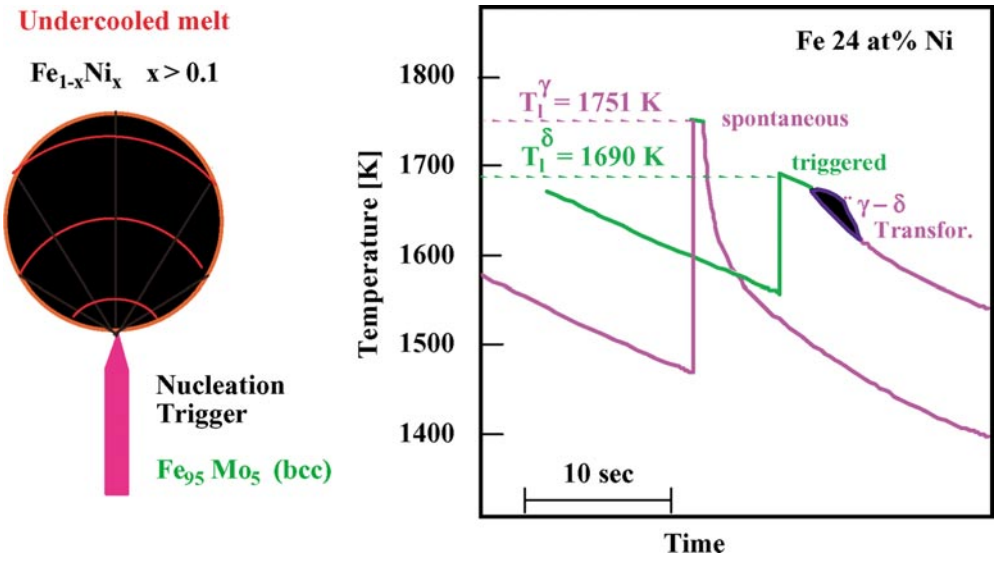

Figure 2. Temperature-time profiles for spontaneous and externally triggered crystallization of undercooled $Fe_{76}Ni_{24}$ sample. During spontaneous crystallization stable fcc phase is formed, but on nucleation triggering by an $Fe_{95}Mo_5$ needle of bcc phase (cf left side) the metastable bcc phase in Fe–Ni alloy is succesfully seeded. The primarily formed metastable bcc phase transforms into stable fcc phase during cooling as indicated by the hump on the respective temperature-time profile.

importance of metalloxides on the solidification behaviour. In the case of Ni–V vanadium oxides are formed which are stable at elevated temperatures above the liquidus temperatures of the metallic Ni–V samples. They show a cubic crystalline structure, being more similar to the fcc and bcc phases than to σ' phase. Therefore, the catalytic potency factor $f(\theta)$ of heterogeneous nucleation due to the vanadium oxides is more pronounced for the nucleation of the cubic phases than of the intermetallic σ' phase [18].

3.3. Phase-selection diagrams

The dependence of the formation of different crystallographic phases on the undercooling obtained prior to solidification is used to develop phase selection diagrams. Such diagrams correspond to phase diagrams, but containing besides the concentration of an alloy also the undercooling as a parameter for the formation of different crystallographic phases. As an example figure 3 depicts the phase selection diagram of the pseudo-binary alloy of isopleth $Fe_{69}Cr_{31-x}Ni_x$ [19].

The solid lines in the phase diagram represent the liquidus and the solidus temperatures as well as the boundary between the austenitic (fcc) and the ferritic (bcc) regime. The squares and triangles denote the primary nucleation of the bcc phase and the fcc phase, respectively. On the left hand side (ferritic regime), bcc solidification is observed to be independent of undercooling. However, on the right hand side (austenitic regime), metastable bcc solidification occurs at undercoolings exceeding a critical value which changes with concentration. The results have been analysed by calculating the activation energy ΔG^* for bcc and fcc solidification according to classical nucleation theory (CNT) and constructing a boundary line under the condition of $\Delta G^*(\text{fcc}) = \Delta G^*(\text{bcc})$. The fair agreement with the experimental results confirms the validity of equation (1).

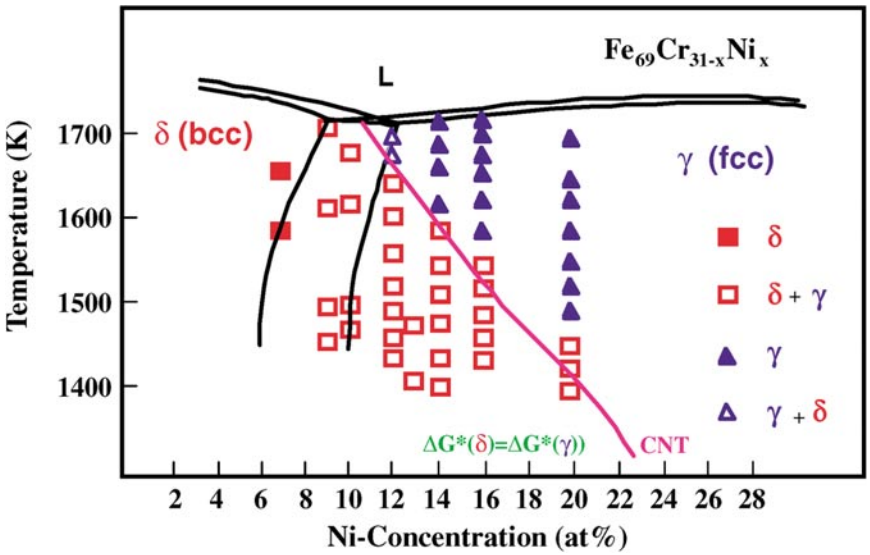

Figure 3. Phase diagram of the quasi-binary alloy $Fe_{69}Cr_{31-x}Ni_x$ showing the results of undercooling experiments; the symbols classify primary nucleation of the bcc (squares) and the fcc (triangles) phases. The curve denoted by CNT corresponds to the phase-boundary line predicted by classical nucleation theory.

The boundary line strongly depends on the Ni composition. This clearly demonstrates that the undercooling is an important processing parameter enabling the solidification of the metastable bcc phase owing to its smaller interface energy σ_{sl} in the regime of the phase diagram where the fcc phase is stable. However, because of the small cooling rates in the levitation experiments, the primarily solidified metastable bcc phase cannot be fully conserved during cooling to ambient temperature since it transforms via a solid-state reaction to the stable fcc phase. The fraction of the metastable phase conserved at room temperature is increased by quenching the solidified sample in a liquid metallic bath [19].

4. Rapid crystal growth in undercooled melts

4.1. Dilute alloys

Nucleation is the first step in the crystallization of undercooled melts, preselecting the crystallographic phase, stable or metastable. Crystallization is completed by subsequent crystal growth. The conditions underlying the solidification of undercooled melts imply dendritic growth, which is described in terms of the growth velocity V, undercooling ΔT and the dendrite tip radius R [20]. The dendrite growth velocity is measured on levitation processed samples as a function of undercooling by means of a high-speed photosensing device [21] or, for high-precision measurements, with a capacity sensor [22].

Figure 4 shows the dendrite growth velocity V as a function of undercooling ΔT as measured for two dilute Ni–B alloys of 0.7 at.% (squares) and 1.0 at.% (circles) boron concentration. The experimental results have been analysed within current theories of dendrite growth following the same procedure as applied in [23]. The results of the calculations are represented by the solid lines in figure 4. For comparison, the (calculated) growth velocity $V(\Delta T)$ for pure Ni is shown (thick solid line). It is obvious that dendrite growth theory is

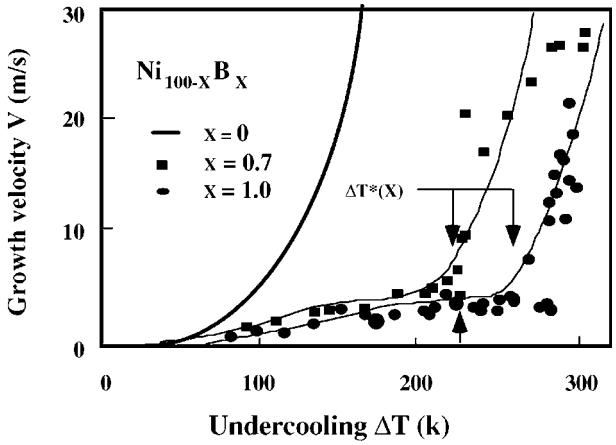

Figure 4. Dendrite growth velocity V as a function of undercooling ΔT measured for a $Ni_{99.3}B_{0.7}$ (squares) and $Ni_{99}B$ (circles). The solid curves represent the predictions of dendrite growth theory. The thick line gives the calculated growth velocity for pure Ni.

able to describe the experimentally determined growth velocity–undercooling relationship in a satisfactory manner, provided a velocity-dependent partition coefficient $k(V)$ [23] is taken into account. The addition of small amounts of boron leads to a drastic reduction of the growth velocity, compared to the pure metal, at undercoolings less than a critical undercooling ΔT^*. The critical undercooling depends very sensitively on the boron concentration. If it is exceeded, the growth velocity sharply increases with undercooling. This behaviour is interpreted as a transition from diffusion-controlled growth to thermally controlled growth. At $\Delta T \approx \Delta T^*$ solute trapping [24] sets in, leading to partitionless solidification at undercoolings $\Delta T > \Delta T^*$. The partitionless solidification at large undercoolings is confirmed by measurements on the as-solidified samples using the method of autoradiography [23]. These investigations clearly reveal the formation of metastable supersaturated alloys from the undercooled melt at large undercoolings $\Delta T > \Delta T^*$. Later on, these results were confirmed by measurements on the similar dilute system Ni–Zr, in which the most important parameter for modelling of dendrite growth, the atomic diffusive speed, V_D, was independently determined by laser surface resolidification experiments in combination with Rutherford backscattering investigations on the as solidified thin layers [25].

4.2. Intermetallics with superlattice structures

A phenomenon quite analogous to solute trapping is disorder trapping. It occurs during rapid solidification in melts of intermetallic compounds which form superlattice structures under equilibrium solidification conditions. Disorder trapping means that the growth velocity is too high to build up the superlattice of the intermetallic phase. It is theoretically described by a model by Boettinger and Aziz [26]. Figure 5 shows the results of measurements on the equiatomic intermetallic compound CoSi [27].

The squares represent the experimental results. Dendrite growth theory is used to analyse the experiments. First, it is assumed that the interface undercooling $\Delta T_k = V/\mu$ (where μ is the kinetic growth coefficient) is determined from the model of collision-limited growth, which sets the speed of sound as the limiting factor of crystal growth [28]. This leads to the dashed line in Figure 5. Apparently, the assumption of the validity of collision-limited growth

overestimates the velocity. Alternatively, diffusion-limited growth is supposed. Under these conditions, the atomic diffusive speed is the limiting factor, and μ is small, which results in a large interface undercooling ΔT_k. The experimental data can be fitted under the assumption of diffusion-limited growth. The best fit is obtained for $\mu = 0.021$ m s^{-1} K^{-1} which is much less than $\mu = 4.2$ m s^{-1} K^{-1} for collision-limited growth. The resulting conclusion is that at undercoolings below a critical undercooling $\Delta T^* \approx 310$ K growth is diffusion limited. This is understood by the fact that the build-up of a superlattice structure requires atomic diffusion over at least two interatomic spacings. Therefore, the diffusive (and not the atomic vibration) frequency is the decisive parameter in this ΔT regime.

However, if the undercooling exceeds a critical value $\Delta T^* \approx 310$ K, the velocity V starts to rise rapidly. The slope of the $V(\Delta T)$ curve beyond the critical undercooling is comparable to that of the curve calculated under the assumption of collision-limited growth. This transition is understood by the onset of disorder trapping at $\Delta T \approx 310$ K, when the growth velocity becomes comparable to, or even larger than, the atomic diffusive speed. The atoms can no longer sort themselves out onto the various sublattices of the intermetallic phase. This leads to a disordered structure. In the present levitation experiments, the cooling rate is too small to avoid reordering of the as-solidified samples. Therefore, the disordered structure, primarily solidified at the largest undercooling, cannot be revealed by, e.g., diffraction studies on the as-solidified material cooled down to room temperature. However, it is evidenced in Ni–Al based intermetallic compounds both by investigations of the solidification velocity versus undercooling relation [29] and transmission electron microscopy (TEM) studies as well [30]. The TEM micrographs clearly show the existence of antiphase domains.

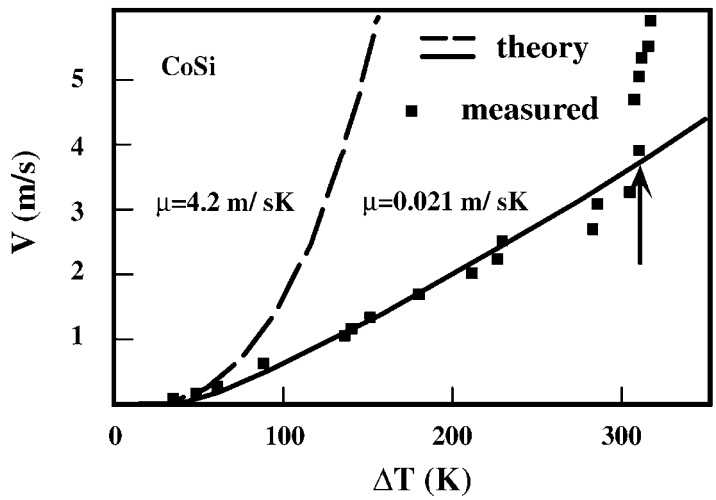

Figure 5. The dendrite growth velocity V as a function of undercooling ΔT for the intermetallic compound CoSi. The squares give the measured velocities. The lines represent the theoretical predictions assuming either collision-limited growth (dashed line) or diffusion-limited growth (solid line).

4.3. Semiconductors

Investigations of the crystal growth in undercooled melts of semiconductors are of special interest and have been performed on pure Ge and pure Si and their alloys as well [31–36]. These substances behave as metals in the liquid state and as semiconductors with strong

covalent bondings in the solid state. Figure 6 shows the crystal growth velocity as a function of undercooling for pure Ge (open triangles), and two dilute Ge–Sn alloys, containing 0.39 at.% Sn (closed circles) and 2 at.% Sn (open squares), respectively [35]. The growth velocity of pure Ge is rather sluggish and reaches 1 m s^{-1} at the highest undercooling of $\Delta T = 426$ K. For comparison, in pure metals the growth velocity is one to two orders of magnitude larger [37]. Surprisingly, the addition of only 0.39 at.% of the metallic element Sn to Ge increases the growth velocity by a factor of five leading to a maximum velocity of 5 m s^{-1} at $\Delta T \approx 400$ K. But a further increase of the Sn concentration to 2 at.% has no essential effect on the growth velocity versus undercooling relation.

The experimental results have been analysed within the frame of dendritic growth assuming the validity of the collision-limited growth model, i.e. $V_o = V_s$, since liquid Ge is metallic and has a structure and coordination number similar to that of the dense random packing characteristic of liquid metals. The atomic attachment factor f is considered to be the essential parameter in describing the growth behaviour in pure Ge and dilute Ge–Sn alloys. It denotes the fraction of interfacial sites at which atomic attachment can occur. This fraction is close to unity for pure metals with a rough solid–liquid interface. But it should be small for the smooth solid-liquid interfaces of tetrahedrally coordinated semiconductors, because these materials, like Ge, are strongly covalently bound. The factor f is used as the only free parameter to describe the crystal growth velocities measured as a function of undercooling on Ge and Ge–Sn alloys within dendrite growth theory. The results of the calculations are represented by the solid lines in figure 6. Also in figure 6, the numerical values of the factor f are given which lead to the best description of the measured data. For pure Ge, $f = 0.01$ results. This is in fair agreement with $f = 0.02$ as determined by laser surface resolidification experiments on pure Si [38] taking into account that Ge is isomorphous with Si. The increase of the growth velocity by the addition of 0.39 at.% Sn implies a larger value, $f = 0.045$. This means that the fraction of interfacial sites at which atomic attachment can occur increases by the addition of the metallic component. Obviously, this effect prevails the counteracting effect of the contribution of the constitutional undercooling, which decreases the growth velocity. This finding is supported by the results on the Ge–2 at.% Sn alloy. Even though f is further increased from $f = 0.045$ to $f = 0.09$ the velocity remains essentially unchanged in comparison with the Ge–0.39 at.% alloy. This means that with increasing Sn concentration the constitutional undercooling becomes more important. Detailed studies of the growth behaviour and its consequences on microstructure evolution indicate that different growth modes are present depending on undercooling. They lead to different microstructures, facetted at small undercoolings, dendritic at medium undercoolings and grain refined at high undercoolings [34, 35].

5. Grain refinement in undercooled melts

Since the pioneering work by Walker [39] it is well known that the phenomenon of grain refinement occurs if the undercooling passes certain critical undercoolings ΔT^*. Liquid metals solidify either into a coarse-grained dendritic microstructure or into a refined equiaxed microstructure [40]. Figure 7 illustrates the development of the microstructure if the undercooling of a $Cu_{70}Ni_{30}$ sample is varied [41]. At small undercoolings a grain refined equiaxed microstructure appears, which changes at a critical undercooling ΔT_1^* to a coarse-grained dendritic microstructure. The grain refined equiaxed microstructure re-enters at a critical undercooling ΔT_2^* and prevails in the large-undercooling range.

Several mechanisms have been discussed to explain the physical origin of the grain refinement at the critical undercoolings [42]. Recently, a model has been developed [43] and experimentally tested [41, 44] which describes the fragmentation of primarily formed

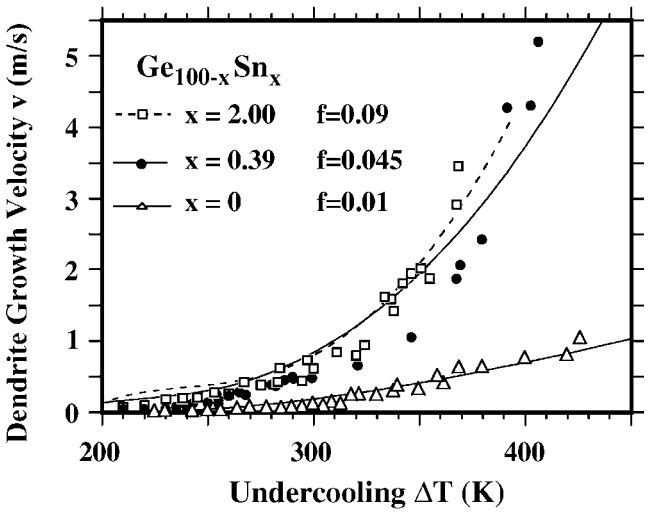

Figure 6. Growth velocity as a function of undercooling for pure Ge and dilute Ge–Sn alloys. The symbols represent the experimentally determined data while the lines give the predictions of dendrite growth theory with f, the atomic impingement factor, as the only free parameter.

dendrites due to a Rayleigh-like instability of the dendritic morphology. This process is driven by the solid/liquid interfacial energy: the system attempts to minimize its interfacial area via heat and solute diffusion in the bulk liquid phase ahead of the solid-liquid interface. The break-up of the dendrites requires a characteristic time, $\Delta t_{bu}(\Delta T)$, which depends on the undercooling. Furthermore, it is assumed that the break-up of the dendrites occurs during the post-recalescence or plateau time Δt_{pl} of a crystallization event, i.e., before the sample has had time to completely solidify. According to this picture, a grain refined equiaxed microstructure is observed if $\Delta t_{bu} < \Delta t_{pl}$, and a coarse-grained microstructure if $\Delta t_{bu} > \Delta t_{pl}$. The break-up time Δt_{bu} is calculated in a first approximation [43] as

$$\Delta t_{bu} \approx \frac{R_{tt}^3}{d_o a_t}\left(1 - \frac{m_l c_o(1-k_E)}{\Delta H_f/C_p}\frac{a_t}{D}\right) \tag{3}$$

with R_{tt} the dendrite trunk radius, $d_o = \Gamma C_p/\Delta H_f$ the capillary length, a_t the thermal diffusivity, Γ the Gibbs–Thomson coefficient, C_p the specific heat of the undercooled melt, ΔH_f the heat of fusion, D_c the chemical diffusion coefficient, m_l the slope of the liquidus line, c_o the nominal solute concentration and k_E the equilibrium partition coefficient.

Figure 8 shows the break-up time as a function of undercooling calculated according to equation (3) using the characteristic data of a $Cu_{70}Ni_{30}$ alloy. The break-up time sharply decreases with undercooling, passes through a minimum, rises very rapidly and finally goes through a maximum before falling again.

The occurrence of a minimum and a maximum in the $\Delta t_{bu}(\Delta T)$ relationship is linked to the dependence on the trunk (or dendrite tip) radius R. At small undercoolings, dendrite growth is controlled mainly by chemical diffusion, and the tip radius decreases as the concentration gradient becomes steeper. As the undercooling is further increased, solute trapping sets in, leading to a decrease of the concentration gradient and an increase of the tip radius until the absolute stability of solutal dendrites is reached. Beyond this limit, dendritic growth is purely thermally controlled, and the radius falls again due to an increase of the thermal gradient.

The three thin solid lines correspond to three series of experiments, each with a different cooling rate. According to the predictions of the model, the intersection points between the

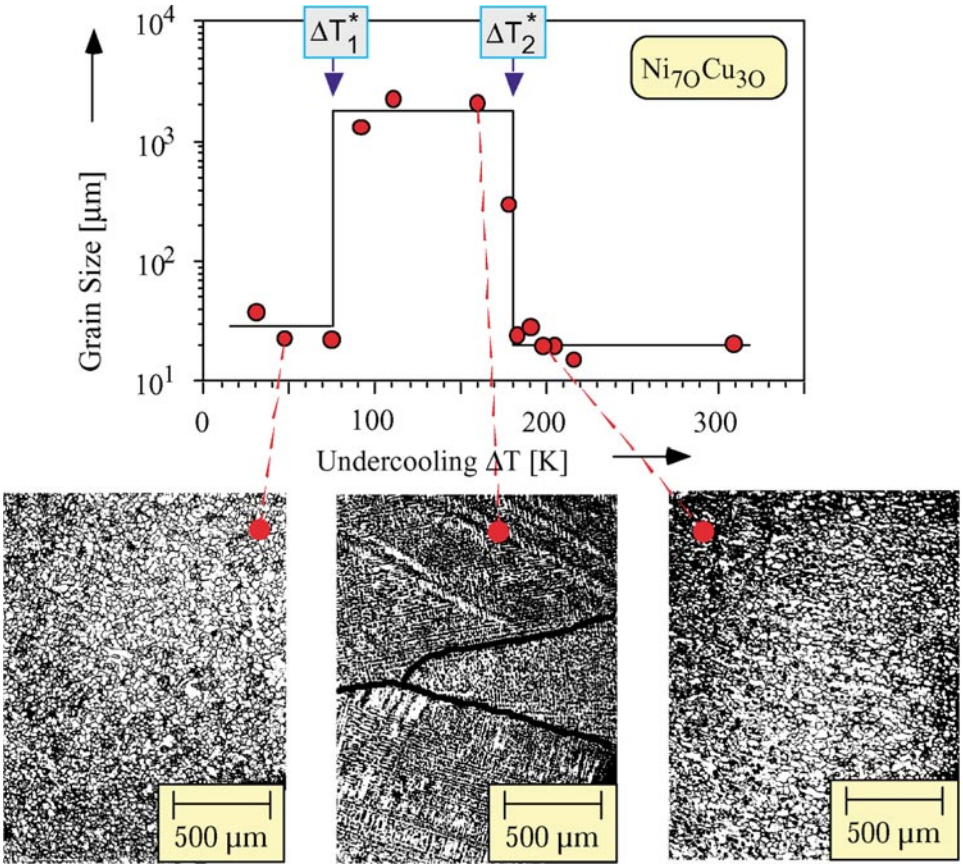

Figure 7. Grain diameter d as a function of undercooling for a $Ni_{70}Cu_{30}$ sample. The photographs show the morphology of the different microstructures.

$\Delta t_{bu}(\Delta T)$ and $\Delta t_{pl}(\Delta T)$ curves define the transitional undercoolings ΔT_1^* and ΔT_2^*. Δt_{pl} should depend on the rate Q at which the latent heat is being transferred from the sample to the environment and, hence, on the rate at which the sample is being cooled. As indicated by the arrows, which mark the transitional undercoolings determined independently from microstructural investigations, there is a good agreement despite some simplifying assumptions made in the model [41]. In particular, the model is able to predict the experimentally observed 'double transition' in the grain size–undercooling relation of alloys, and the dependence of the critical undercooling ΔT_2^* both on cooling rate and alloy composition [44].

6. Magnetic order in undercooled metallic melts

The foregoing experiments have shown that metallic elements are undercooled by considerable amounts through the application of the electromagnetic levitation. This raises the question of whether a material could be undercooled below its Curie temperature T_C to study magnetic ordering in a liquid system. So far it is well known that ordered magnetic phases are restricted to occur exclusively in solid matter.

Therefore, we have attempted to undercool a metallic alloy which shows ferromagnetic

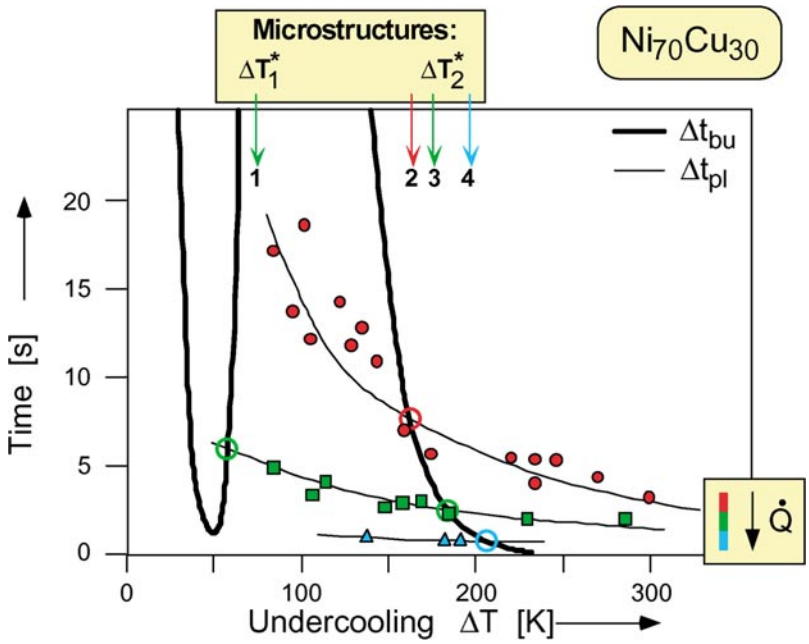

Figure 8. Calculated dendrite break-up time Δt_{bu} (thick solid line) and post-recalescence time Δt_{pl} (thin solid lines) as a function of undercooling ΔT. The symbols denote the post-recalescence times Δt_{pl} versus undercooling determined from the measured temperature-time profiles for three different cooling rates.

ordering in the solid state by the use of electromagnetic levitation technique. As the most suitable alloy system we have chosen the binary alloy $Co_{80}Pd_{20}$.This alloy was selected for the present studies because it shows the highest relative Curie temperature $T_{rC} = T_C/T_m$ (T_m: melting temperature) and because the Co–Pd alloy system is completely miscible over the entire concentration range. Figure 9 shows a temperature-time profile as measured on a levitation undercooled sample of $Co_{80}Pd_{20}$ [45]. The dashed line represents the Curie temperature of the solid ferromagnet and the dashed line denoted by Tu gives the Curie temperature of the liquid ferromagnet. The latter was obtained by measurements of the temperature dependence of the magnetic susceptibility on the levitation undercooled alloy [46]. It is obvious that the sample could be undercooled to temperatures quite close to the Curie temperature of the liquid ferromagnet. In such a case even the hypercooling limit was exceeded [47]. At such temperatures an attractive force between the undercooled melt and an external strong permanent magnet of CoSm was clearly detected.

A modified Faraday balance was utilized to measure the magnetic susceptibility as a function of the temperature in the liquid undercooled regime. Figure 10 shows the reciprocal magnetic susceptibility as a function of temperature, measured for a $Co_{80}Pd_{20}$ alloy in the solid (crosses) and undercooled liquid (dots) state. The insert gives the rapid increase of the magnetization of the liquid sample if the temperature approaches the Curie temperature [46]. The liquid sample shows a similar behaviour to the solid sample. The slopes of both lines are similar. Apparently, the magnetic moments of the liquid and solid ferromagnets are comparable, indicating similar magnetic moments in the liquid and solid material. The only difference is that the extrapolation of the data to $1/\chi = 0$ leads to a Curie temperature of the liquid ferromagnet which is smaller by about 20 K than that of the solid ferromagnet. The

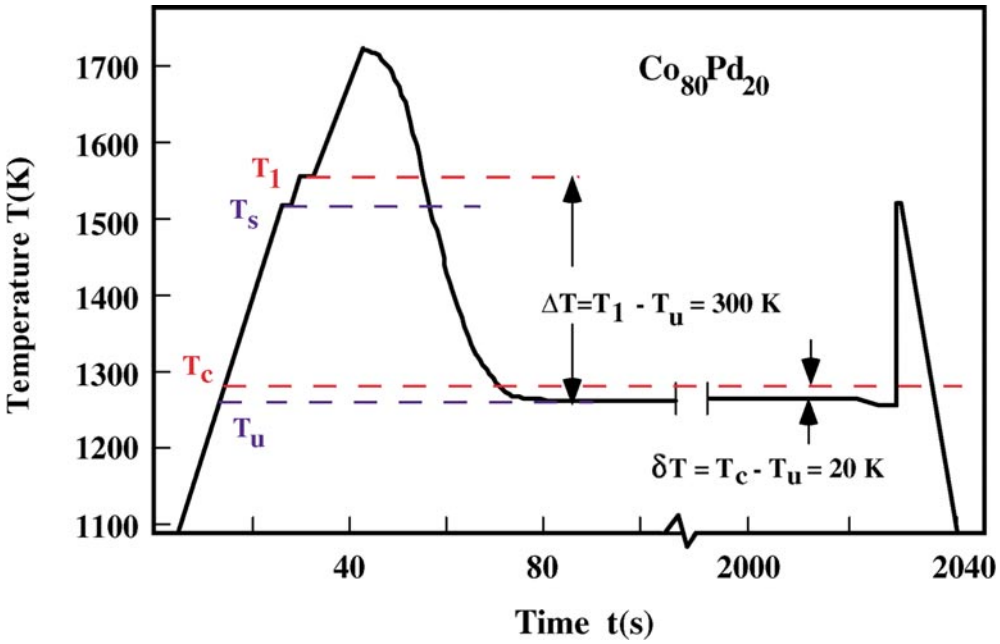

Figure 9. Temperature-time profile as measured on a levitation undercooled $Co_{80}Pd_{20}$ alloy. The dashed line labelled T_C represents the ferromagnetic Curie temperature of the solid material while the dashed line labelled T_u gives the respective Curie temperature of the liquid ferromagnet.

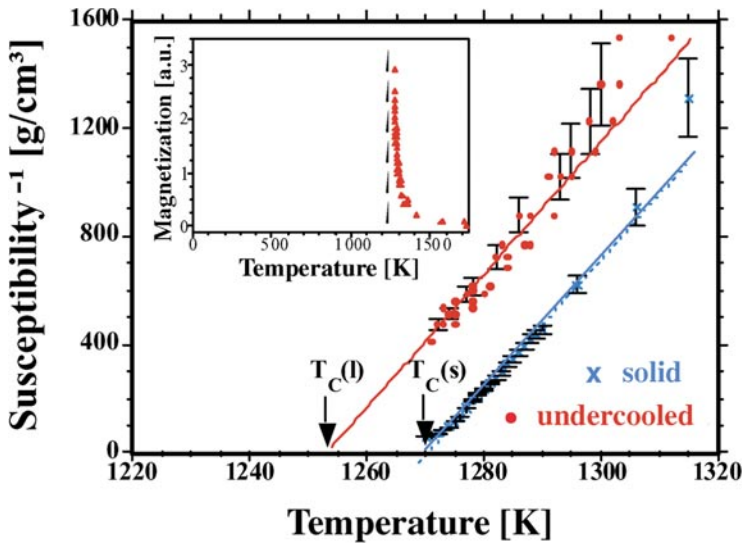

Figure 10. Reciprocal magnetic susceptibility as a function of temperature, measured for a $Co_{80}Pd_{20}$ alloy in the solid (crosses) and undercooled liquid (dots) state. The insert gives the rapid increase of the magnetization of the liquid sample if the temperature approaches the Curie temperature.

results of the measurements of the macroscopic volume susceptibility using the method of the Faraday balance coincide with measurements of the microscopic susceptibility applying

the muon-spin-rotation (μSR) technique [48]. The similar behaviour of the liquid and solid ferromagnets is understood if it is assumed that the Curie temperature is mainly determined by the exchange interaction, which depends on the interatomic distance. This result is then not surprising since the change of the mass density is only 4% during melting. Also, the relaxation times of the spin system are much shorter than the structural relaxation times. This means that the dynamic behaviour of the magnetic spin system does not differ between solid and liquid states.

So far, with the exception of one work [49] it was not possible to undercool Co–Pd alloys below their Curie temperature [50]. In contrast studies of the concentration dependence and the nucleation statistics of Co–Pd melts rather suggest that the onset of magnetic ordering in the undercooled melts stimulates crystal nucleation [51]. Magnetic ordering may initiate crystallization of undercooled melts in some analogy to magnetically driven phase transformations in solids, e.g. the α–γ-transformation in pure Fe or Fe–Ni alloys.

7. Summary and conclusions

The undercooling and solidification of metallic melts have been experimentally studied. Several critical undercoolings for various non-equilibrium solidification phenomena were identified as (i) the nucleation of a metastable phase with a crystallographic structure different from that of the stable counterpart, (ii) the onset of solute and disorder trapping, being important for the formation of metastable supersaturated solutions and disordered intermetallic phases, and (iii) the solidification of grain refined equiaxed microstructures. The latter one has been successfully described by a model developed by Karma [43]. Very recent findings on the formation of an undercooled metallic melt with long-range magnetic order have been reported.

Acknowledgments

The author expresses his sincere gratitude to M Barth, K Eckler, D Holland-Moritz, D Li, C Notthoff, D Platzek, J Schroers, M Schwarz, T Volkmann and B Wei for their invaluable work to obtain the results presented. Part of this work was financially supported by the 'Deutsche Forschungsgemeinschaft', the 'Deutsche Agentur für Raumfahrtangelegenheiten' and the 'European Communities'.

References

[1] See e.g. Herlach D M, Egry I, Baeri P and Spaepen F (eds) 1994 *Undercooled Metallic Melts: Properties, Solidification and Metastable Phases (Proc. NATO ARW) (Il Ciocco, 1993); Mater. Sci. Eng.* A **178** (1/2)
[2] Herlach D M, Cochrane R F, Egry I, Fecht H-J and Greer A L 1993 *Int. Mater. Rev.* **38** 273
[3] Christian J W 1975 *The Theory of Transformation in Metals and Alloys* (Oxford: Pergamon)
[4] Spaepen F 1975 *Acta Metall.* **23** 729
[5] Frank F C 1952 *Proc. R. Soc.* A **215** 43
[6] Turnbull D 1952 *J. Chem. Phys.* **20** 411
[7] Holland-Moritz D, Herlach D M and Urban K 1993 *Phys. Rev. Lett.* **71** 1196
[8] Holland-Moritz D, Schroers J, Herlach D M, Grushko B and Urban K 1998 *Acta Mater.* **46** 1601–15
[9] Schaefer R J, Benderski L A and Biancaniello F S 1987 *J. Physique* **47** 311
[10] Herlach D M, Gillessen F, Volkmann Th, Wollgarten M and Urban K 1992 *Phys. Rev.* B **46** 5203
[11] Herlach D M, Feuerbacher B and Schleip E 1991 *Mater. Sci. Eng.* A **133** 795
[12] Schleip E, Herlach D M and Feuerbacher B 1990 *Europhys. Lett.* **11** 751
[13] Löser W, Volkmann T and Herlach D M 1994 *Mater. Sci. Eng.* A **178** 163
[14] Volkmann T, Löser W and Herlach D M 1997 *Metall. Mater. Trans.* A **28** 453–70
[15] Schroers J, Volkmann T, Herlach D M, Allen D R and Perepezko J H 1996 *Int. J. Rapid Solidification* **9** 267

[16] Holland-Moritz D 1998 *Int. J. Non-Equilibrium Processing* **11** 169
[17] Notthoff C, Franz H, Hanfland M, Herlach D M, Holland-Moritz D and Petry W 2000 *Rev. Sci. Instrum.* **71** 3791
[18] Notthoff C, Feuerbacher B, Frans H, Herlach D M and Holland-Moritz D 2001 *Phys. Rev. Lett.* **86** 1038
[19] Löser W, Garcia-Escorial A and Vinet B 1998 *Int. J. Non-Equilibrium Processing* **11** 87
[20] See e.g. Kurz W and Fisher D J 1989 *Fundamentals of Solidification* (Aedermannsdorf: Trans Tech)
[21] Schleip E, Willnecker R, Herlach D M and Görler G P 1988 *Mater. Sci. Eng.* A **98** 39
[22] Eckler K and Herlach D M 1994 *Mater. Sci. Eng.* A **178** 159
[23] Eckler K, Cochrane R F, Herlach D M, Feuerbacher B and Jurisch M 1992 *Phys. Rev.* B **45** 5019
[24] Aziz M J 1982 *J. Appl. Phys.* **53** 1158
[25] Arnold C B, Aziz M J, Schwarz M and Herlach D M 1999 *Phys. Rev.* B **59** 334
[26] Boettinger W J and Aziz M J 1989 *Acta Metall.* **37** 3379
[27] Barth M, Wei B and Herlach D M 1995 *Phys. Rev.* B **51** 3422
[28] Turnbull D 1982 *Acta Metall.* **30** 2135
[29] Goetzinger R, Barth M, Herlach D M, Hunziker O and Kurz W 1997 *Mater. Sci. Eng.* A **226–228** 415
[30] Assadi H, Barth M, Greer A L and Herlach D M 1996 *Mater. Sci. Forum* **215/216** 37–44
[31] Li D, Volkmann T, Eckler K and Herlach D M 1995 *J. Cryst. Growth* **152** 101
[32] Li D, Eckler K and Herlach D M 1995 *Europhys. Lett.* **32** 223
[33] Li D and Herlach D M 1996 *Europhys. Lett.* **34** 423
[34] Li D, Eckler K and Herlach D M 1996 *Acta Mater.* **44** 2437
[35] Li D and Herlach D M 1996 *Phys. Rev. Lett.* **77** 1801
[36] Li D and Herlach D M 1997 *J. Mater. Sci.* **32** 1437
[37] Willnecker R, Herlach D M and Feuerbacher B 1989 *Phys. Rev. Lett.* **62** 2709
[38] Spaepen F and Turnbull D 1982 *Laser Annealing of Semiconductors* ed J M Poate and J W Mayer (New York: Academic) p 15
[39] Walker J L 1959 *The Physical Chemistry of Process Metallurgy* ed G R St Pierre (New York: Interscience) pt 2, p 845
[40] For an overview, see Munitz A and Abbaschian R 1986 *Undercooled Alloy Phases* ed E W Collings and C C Koch (Warrendale, PA: AIME) p 23
[41] Schwarz M, Karma A, Eckler K and Herlach D M 1994 *Phys. Rev. Lett.* **73** 1380
[42] See e.g. the review Herlach D M 1994 *Mater. Sci. Eng.* R **12** 177
[43] Karma A 1998 *Int. J. Non-Equilibrium Processing* **11** 201
[44] Eckler K, Schwarz M, Karma A and Herlach D M 1996 *Mater. Sci. Forum* **215/216** 45
[45] Platzek D, Notthoff C, Herlach D M, Jacobs G, Herlach D and Maier K 1994 *Appl. Phys. Lett.* **65** 1723
[46] Reske J, Herlach D M, Keuser F, Maier K and Platzek D 1995 *Phys. Rev. Lett.* **75** 737
[47] Volkmann T, Wilde G, Willnecker R and Herlach D M 1998 *J. Appl. Phys.* **83** 3028
[48] Herlach D, Bührer K, Herlach D M, Maier K, Notthoff C, Platzek D and Reske J 1998 *Europhys. Lett.* **44** 98
[49] Albrecht T, Bührer C, Fähnle M, Maier K, Platzek D and Reske J 1997 *Appl. Phys.* A **65** 215
[50] Herlach D M, Holland-Moritz D, Schenk Th, Schneider K, Wilde G, Boni F, Fransaer J and Spaepen F 1999 *J. Non-Cryst. Solids* **250–252** 271
[51] Schenk T, Holland-Moritz D and Herlach D M 2000 *Europhys. Lett.* **50** 402